# Intermolecular interactions-photophysical properties relationships in phenanthrene-9,10-dicarbonitrile assemblies

Afanasenko, Anastasiia M.; Novikov, Alexander S.; Chulkova, Tatiana G.; Grigoriev, Yakov M.; Kolesnikov, Ilya E.; Selivanov, Stanislav; Starova, Galina L.; Zolotarev, Andrey A.; Vereshchagin, Anatoly N.; Elinson, Michail N.

*Published in:*
Journal of Molecular Structure

*DOI:*
10.1016/j.molstruc.2019.07.036



*Publication date:*
2020

Journal of Molecular Structure 1199 (2020) 126789

Contents lists available at ScienceDirect

Journal of Molecular Structure

journal homepage: http://www.elsevier.com/locate/molstruc

# Intermolecular interactions-photophysical properties relationships in phenanthrene-9,10-dicarbonitrile assemblies

Anastasiia M. Afanasenko [a, b], Alexander S. Novikov [a], Tatiana G. Chulkova [a, *], Yakov M. Grigoriev [a], Ilya E. Kolesnikov [a], Stanislav I. Selivanov [a], Galina L. Starova [a], Andrey A. Zolotarev [a], Anatoly N. Vereshchagin [c], Michail N. Elinson [c]

[a] Saint Petersburg State University, 7/9 Universitetskaya Nab., Saint Petersburg, 199034, Russia
[b] Stratingh Institute for Chemistry, University of Groningen, Nijenborgh 4, 9747 AG, Groningen, the Netherlands
[c] N. D. Zelinsky Institute of Organic Chemistry, 47 Leninsky Prospect, Moscow, 119991, Russia

ARTICLE INFO

*Article history:*
Received 26 May 2019
Received in revised form
1 July 2019
Accepted 7 July 2019
Available online 30 August 2019

*Keywords:*
Phenanthrene-9,10-dicarbonitriles
DFT studies
Fluorescence
π-Stacking

ABSTRACT

Phenanthrene-9,10-dicarbonitriles show various luminescence behaviour in solution and in the solid state. Aggregation patterns of phenanthrene-9,10-dicarbonitriles govern their luminescent properties in the solid state. Single crystal structures of phenanthrene-9,10-dicarbonitriles showed head-to-tail intraplane (or quasi-intraplane) intermolecular interactions and π-stacking patterns with eclipsing of molecules when viewed orthogonal to the stacking plane. The π-stacking interactions were detected in the X-ray structures of phenanthrene-9,10-dicarbonitriles and studied by DFT calculations at the M06−2X/6−311++G(d,p) level of theory and topological analysis of the electron density distribution within the framework of QTAIM method. The estimated strength of the C···C contacts responsible for the π-stacking interactions is 0.6−1.1 kcal/mol. The orientation of molecules in crystals depends on the substituents in phenanthrene-9,10-dicarbonitriles. Distinct molecular orientation and packing arrangements in crystalline phenanthrene-9,10-dicarbonitriles ensured perturbed electronic communication among the nearest and non-nearest molecules through an interplay of excimer and dipole couplings. As a result, the intermolecular interactions govern the solid state luminescence of molecules.



## 1. Introduction

Luminescent compounds attract great attention as objects for their potential applications in various research fields, including organic light-emitting diodes (OLEDs), luminescent sensors, surface coatings, inks, *etc.* [1–3] The aggregation patterns of luminescent compounds can influence their absorption and emission properties. It is known, that photophysical properties of fused aromatic compounds such as anthracene, pyrene, and benzocoumarins depend greatly on their aggregation state. For example, anthracene, pyrene, and methyl 8-(dimethylamino)-2-oxo-2H-benzo[g]chromene-3-carboxylate possess strong fluorescence in solution, but have poor emission in the solid state [4–6]. However, cyanine-based dyes, perylene diimides, methyl 9-(dimethylamino)-3-oxo-3H-benzo[f]chromene-2-carboxylate and porphyrins show the opposite luminescence behaviour [6–15]. Congruently, investigations into the structure−packing−optical property relationship in molecular aggregates have received much attention from theoretical and experimental views. Most applications of Frenkel exciton theory in molecular aggregate photophysics employ the point-dipole approximation for the Coulomb coupling between two neighbouring molecules,

$$J_C = \frac{\mu^2(1 - 3\cos^2\theta)}{4\pi\varepsilon R^3}$$

where μ is the dipole moment corresponding to the $S_0 \rightarrow S_1$ transition of two neighbouring molecules, respectively, R is the displacement vector connecting the molecular mass centres, and $\varepsilon$ is the dielectric constant of the medium. The case for parallel transition dipole moments, which characterizes packing geometries with one molecule per unit cell, is depicted in Fig. 1.

Kasha initially identified two aggregation species based on the relative orientation of molecules, which is determined by the angle

* Corresponding author.
*E-mail address:* t.chulkova@spbu.ru (T.G. Chulkova).

https://doi.org/10.1016/j.molstruc.2019.07.036
0022-2860/

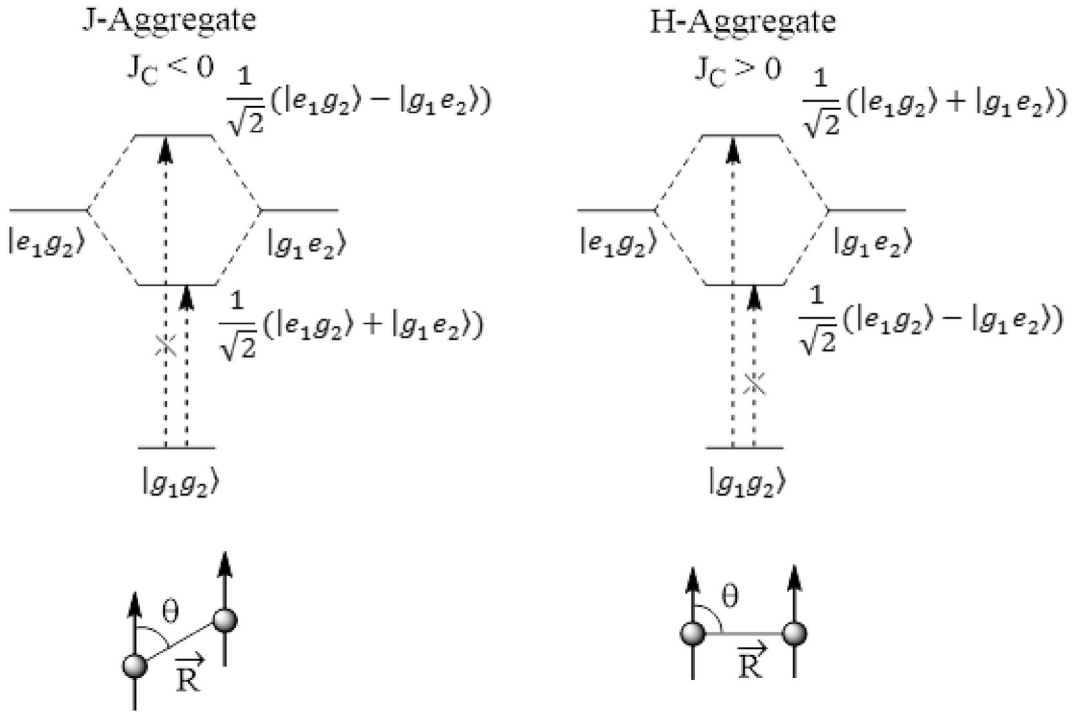


**Fig. 1.** Relative orientation of transition dipole moments defining a J-aggregate ($\theta < \theta M$) and H-aggregate ($\theta M < \theta < \pi/2$) under the point dipole approximation. The magic angle θM is 54.7°. Energy level diagrams for J- and H-aggregate dimers. Transitions from the ground state are allowed only to the state with in-phase transition dipole moments, which lie at the bottom and top of the band in J- and H-aggregates, respectively. The symmetric splitting observed in both cases is $2|J_C|$.

θ in Fig. 1. In what is known as J-aggregates, the dipoles maintain a "head-to-tail" orientation where θ is less than the so-called "magic angle" $\theta_M = 54.7°$, the angle for which $J_C$ is zero. In this case, the Coulomb coupling is negative ($J_C < 0$). Conversely, H-aggregates maintain a "side-by-side" orientation ($\theta_M < \theta \leq \pi/2$) leading to a positive Coulomb coupling ($J_C > 0$). As shown by Kasha and co-workers, the sign of the Coulomb coupling has a direct bearing on the photophysical response. This is depicted in Fig. 1 for the simplest case of a molecular dimer, where the Coulomb coupling $J_C$ leads to the formation of two delocalized excited states split by $2|J_C|$. The two states consist of in- and out-of-phase linear combinations of the two local excited states, $|e_1g_2\rangle$ and $|g_1e_2\rangle$. The in-phase or symmetric state, shifted by $J_C$, is characterized by an enhanced transition dipole moment relative to the monomer (by $\sqrt{2}$), whereas the out-of-phase state, shifted by $-J_C$, is optically dark due to a cancellation of the transition dipole moments. Hence, in J-aggregates, the negative coupling ($J_C < 0$) results in the (absorbing) symmetric state having lower energy than the anti-symmetric state, whereas in H-aggregates with $J_C > 0$, the ordering is reversed. The Coulomb-induced energetic shifts lead to predictable changes in the absorption spectrum: in J-aggregates, the main absorption peak is red-shifted compared to the monomer, whereas in H-aggregates, the absorption peak is blue-shifted.

Employing the exciton theory of Davydov, McRae and Kasha surmised that in certain aggregates, which are known as H-aggregates, the Coulomb coupling is positive, resulting in a band of singlet states (excitons) in which the highest energy state consumes all of the oscillator strength. Since in many cases fluorescence proceeds from the lowest excited state (Kasha's rule), fluorescence is suppressed [3].

In contrast, when the Coulomb coupling is negative, as in J-aggregates or Scheibe aggregates, the oscillator strength is focused in the lowest energy exciton, and no suppression of fluorescence is expected.

Also, cofacial molecular assemblies with efficient π-orbital overlap can lead to excited dimers or multimers [16–18]. Excimers are undesired due to dramatic fluorescence quenching. As a result, the fluorescence emission can be tuned, depending on the extent of π -orbital overlap between the molecules [18–20]. The exact impact of short- (orbital overlap mediated excimer) and long-range (Coulomb/dipole) couplings on the optical properties of a molecular ensemble demands special attention [21].

In this work, we studied photophysical properties of substituted 9,10-dicyanophenanthrenes in solution and in the solid state. This study demonstrates the potential of molecular shape control for the development of solid-state luminescent materials.

## 2. Experimental

### 2.1. Materials and methods

All solvents were dried and purified by conventional methods and were freshly distilled under argon shortly before use. Other reagents were used without further purification. FTIR spectra were recorded on Shimadzu FTIR-8400S ($4000-400\,cm^{-1}$) and IRAffinity-1 ($4000-350\,cm^{-1}$) spectrometers using KBr pellets. $^1H$ and $^{13}C$ NMR measurements were performed on a Bruker-DPX 400 instrument at ambient temperature. Electrospray ionization mass spectra were obtained on a Bruker micrOTOF spectrometer equipped with electrospray ionization (ESI) source using MeOH as the solvent. The instrument was operated in both positive and negative ion modes using a *m/z* range of 50–3000. The capillary voltage of the ion source was set at −4500 V ($ESI^+$ −MS) and the capillary exit at ±(70–150) V. The nebulizer gas flow was 0.4 bar and drying gas flow 4.0 L/min. The absorption spectra were recorded on a PerkineElmer precision spectrophotometer Lambda 1050. The emission spectra, excitation spectra, measurements of the lifetimes of excited states were measured on a modular spectrofluorimeter

Fluorolog-3 (Horiba Jobin Yvon). Fluorescence lifetime measurements are based on time-correlated single photon counting (TCSPC). The device also includes an integrating sphere Quanta-φ with fiber optics which enables direct measurement of quantum yields of luminescence.

### 2.2. Synthetic procedures

Phenanthrene-9,10-dicarbonitriles (**1**–**7**) were synthesized starting from commercially available phenylacetonitriles by two step reaction. The synthetic scheme is shown in Fig. 2. Starting from a series of arylacetonitriles, following Linstead's procedure [22,23], the nitriles of 2,3-diarylbutenedioic acids (where aryl is phenyl, 4-fluorophenyl, 4-methylphenyl, and 4-methoxyphenyl) were produced (See the Supporting Information). 2,3-Di(4-chlorophenyl) fumaronitrile, 2,3-di(3,4-dichlorophenyl)fumaronitrile, and 2,3-di(4-bromophenyl)fumaronitrile were produced electrochemically from the appropriate arylacetonitriles (See the Supporting Information) [24]. 2,3-Diarylbutenedioic acid dinitriles were converted to the corresponding 9,10-dicyanophenanthrenes **1**–**7** under UV-irradiation of chloroform solution at the presence of small amounts of iodine [25].

#### 2.2.1. General procedure for the synthesis of phenanthrene-9,10-dicarbonitriles (*1*–*7*)

A chloroform (70 mL) solution of 2,3-diarylbutenedioic acid dinitrile (150 mg) and iodine (several crystals) was irradiated in a quartz flask with a 450 W high pressure mercury lamp for 8 h. After the solvent was evaporated, the residual product was recrystallized from ethanol.

#### 2.2.2. Phenanthrene-9,10-dicarbonitrile (*1*)

Yield: 65 mg (44%), beige powder, mp = 290–291 °C (mp = 290–291 °C [26]). $^1$H NMR (400 MHz, $CDCl_3$) δ, ppm: 8.79 (dd, $^3J$ = 8.4 Hz, $^4J$ = 1.2 Hz, 2H, $H^4$, $H^5$), 8.42 (dd, $^3J$ = 8.4 Hz, $^4J$ = 1.2 Hz, 2H, $H^1$, $H^8$), 7.96 (ddd, $^3J$ = 8.4 Hz, $^3J$ = 7.2 Hz, $^4J$ = 1.2 Hz, 2H, $H^3$, $H^6$), 7.82 (ddd, $^3J$ = 8.4 Hz, $^3J$ = 7.2 Hz, $^4J$ = 1.2 Hz, 2H, $H^2$, $H^7$). $^1$H NMR (400 MHz, DMSO-$d_6$) δ, ppm: 9.11 (dd, $^3J$ = 8.4 Hz, $^4J$ = 1.2 Hz, 2H, $H^4$, $H^5$), 8.32 (dd, $^3J$ = 8.4 Hz, $^4J$ = 1.2 Hz, 2H, $H^1$, $H^8$), 8.08 (ddd, $^3J$ = 8.4 Hz, $^3J$ = 7.6 Hz, $^4J$ = 1.2 Hz, 2H, $H^3$, $H^6$), 8.01 (ddd, $^3J$ = 8.4 Hz, $^3J$ = 7.6 Hz, $^4J$ = 1.2 Hz, 2H, $H^2$, $H^7$). $^{13}$C{$^1$H} NMR (100 MHz, $CDCl_3$) δ, ppm: 131.3, 131.2 ($C^3$, $C^6$), 129.2 ($C^2$, $C^7$), 127.8, 127.4 ($C^1$, $C^8$), 123.4 ($C^4$, $C^5$), 116.8, 115.0 (CN). Using the COSY and $^1$H–$^{13}$C HSQC techniques, assignment of the $^1$H and $^{13}$C NMR signals is achieved (See the Supporting Information). HRMS (ESI$^+$), *m/z*: 229.0760 [M+H]$^+$, 251.0580 [M+Na]$^+$. $C_{16}H_9N_2$ calcd. *m/z*: 229.0766, $C_{16}H_8N_2Na$ calcd. *m/z*: 251.0585. IR spectrum (KBr, selected bands, cm$^{-1}$): 2226 s ν(C≡N), 1608 m ν(CC$_{Ar}$).

#### 2.2.3. 3,6-Difluorophenanthrene-9,10-dicarbonitrile (*2*)

Yield: 54 mg (36%), beige powder, mp = 290–291 °C (291 °C from Ref. [27]). $^1$H NMR (400 MHz, $CDCl_3$) δ, ppm: 8.46 (dd, $^3J_{HF}$ = 9.60 Hz, $^4J_{HH}$ = 2.0 Hz, 2H, $H^4$, $H^5$), 8.27 (dd, $^3J_{HH}$ = 8.2 Hz, $^4J_{HF}$ = 2.4 Hz, 2H, $H^1$, $H^8$), 7.69 (ddd, $^3J_{HF}$ = 9.60 Hz, $^3J_{HH}$ = 8.2 Hz, $^4J_{HH}$ = 2.0 Hz, 2H, $H^2$, $H^7$). $^1$H NMR (400 MHz, DMSO-$d_6$) δ, ppm: 8.94 (dd, $^3J_{HF}$ = 11.2 Hz, $^4J_{HH}$ = 2.4 Hz, 2H, $H^4$, $H^5$), 8.35 (dd, $^3J_{HH}$ = 8.4 Hz, $^4J_{HF}$ = 2.4 Hz, 2H, $H^1$, $H^8$), 7.93 (ddd, $^3J_{HF}$ = 11.2 Hz, $^3J_{HH}$ = 8.4 Hz, $^4J_{HH}$ = 2.4 Hz, 2H, $H^2$, $H^7$). $^{13}$C{$^1$H} NMR (100 MHz, $CDCl_3$) δ, ppm: 164.0 (d, $^1J_{CF}$ = 254.0 Hz, $C^3$, $C^6$), 132.8 (d, $^3J_{CF}$ = 13.0 Hz), 130.3 (d, $^3J_{CF}$ = 10.0 Hz), 124.8, 119.4 (d, $^2J_{CF}$ = 24.0 Hz), 115.7, 114.7, 109.2 (d, $^2J_{CF}$ = 23.0 Hz). HRMS (ESI$^+$), *m/z*: 265.0572 [M+H]$^+$, 287.0391 [M+Na]$^+$. $C_{16}H_7N_2F_2$ calcd. *m/z*: 265.0577. $C_{16}H_6N_2F_2Na$ calcd. *m/z*: 287.0397. IR spectrum (KBr, selected bands, cm$^{-1}$): 3096 m ($C_{sp2}$–H), 2230 s ν(C≡N), 1620, 1524 s ν(CC$_{Ar}$). $^1$H NMR (400 MHz, DMSO-$d_6$) and IR (KBr) spectra are comparable with those reported by E. M. Maya et al. [27].

#### 2.2.4. 3,6-Dichlorophenanthrene-9,10-dicarbonitrile (*3*)

Yield: 47 mg (32%), beige powder, mp = 243–244 °C. $^1$H NMR (400 MHz, $CDCl_3$) δ, ppm: 8.85 (d, $^4J$ = 2.0 Hz, 2H, $H^4$, $H^5$), 8.29 (d, $^3J$ = 8.0 Hz, 2H, $H^1$, $H^8$), 8.02 (dd, $^3J$ = 8.0 Hz, $^4J$ = 2.0 Hz, 2H, $H^2$, $H^7$). $^{13}$C{$^1$H} NMR (100 MHz, $CDCl_3$) δ, ppm: 133.3, 132.7, 131.3, 128.8, 126.8, 126.4, 116.7, 114.4. HRMS (ESI$^+$), *m/z*: 318.9800 [M+Na]$^+$. $C_{16}H_6N_2Cl_2Na$ calcd. *m/z*: 318.9806. IR spectrum (KBr, selected bands, cm$^{-1}$): 3090 w ν($C_{sp2}$–H), 2220 m ν(C≡N), 1599, 1489 s ν(CC$_{Ar}$).

#### 2.2.5. 2,3,5,6-Tetrachlorophenanthrene-9,10-dicarbonitrile (*4*)

Along with **4**, 2,3,6,7-tetrachlorophenanthrene-9,10-dicarbonitrile (**4′**) was obtained as a by-product. Pure compound **4** was prepared by recrystallization from chloroform/acetone solvent mixture. Yield: 57 mg (38%), white powder. $^1$H NMR (400 MHz, $CDCl_3$) δ, ppm: 10.12 (s, 1H), 8.54 (s, 1H), 8.35 (d, $^3J$ = 8.8 Hz, 1 H), 8.02 (d, $^3J$ = 8.8 Hz, 1H). $^{13}$C{$^1$H} NMR (100 MHz, $CDCl_3$) δ, ppm: IR spectrum (KBr, selected bands, cm$^{-1}$): 3146 w ν($C_{sp2}$–H), 2232 m ν(C≡N), 1582, 1472 s ν(CC$_{Ar}$).

#### 2.2.6. 2,3,6,7-Tetrachlorophenanthrene-9,10-dicarbonitrile (*4′*)

$^1$H NMR (400 MHz, $CDCl_3$) δ, ppm: 9.52 (s, 2H), 8.40 (s, 2H).

#### 2.2.7. 3,6-Dibromophenanthrene-9,10-dicarbonitrile (*5*)

Yield: 45 mg (30%), beige powder, mp = 265–266 °C. $^1$H NMR (400 MHz, $CDCl_3$) δ, ppm: 8.67 (s, 2H, $H^4$, $H^5$), 8.37 (d, $^3J$ = 8.0 Hz, 2H), 7.88 (d, $^3J$ = 8.0 Hz, 2H). $^{13}$C{$^1$H} NMR (100 MHz, $CDCl_3$) δ, ppm: 138.4, 131.3, 130.6, 128.9, 126.5, 123.3, 116.5, 114.5. HRMS (ESI$^+$), *m/z*: 384.8970 [M+H]$^+$. $C_{16}H_7N_2Br_2$ calcd. *m/z*: 384.8976. IR spectrum (KBr, selected bands, cm$^{-1}$): 3097 w ν($C_{sp2}$–H), 2230 m ν(C≡N), 1603, 1502 s ν(CC$_{Ar}$).

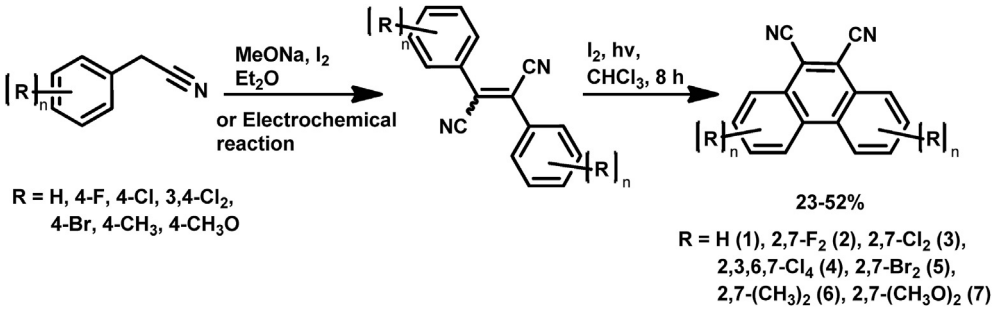


**Fig. 2.** Synthesis of phenanthrene-9,10-dicarbonitriles.

*2.2.8. 3,6-Dimethylphenanthrene-9,10-dicarbonitrile (**6**)*

Yield: 78 mg (52%), beige powder, mp = 246–247 °C. $^1$H NMR (400 MHz, $CDCl_3$) $\delta$, ppm: 8.48 (s, 2H, $H^4$, $H^5$), 8.18 (d, $^3J$ = 8.0 Hz, 2H, $H^1$, $H^8$), 7.64 (d, $^3J$ = 8.0 Hz, 2H, $H^2$, $H^7$), 2.71 (s, 6H, $CH_3$). $^1$H NMR (400 MHz, DMSO-$d_6$) $\delta$, ppm: 8.86 (s, 2H, $H^4$, $H^5$), 8.14 (d, $^3J$ = 8.0 Hz, 2H, $H^1$, $H^8$), 7.81 (d, $^3J$ = 8.0 Hz, 2H, $H^2$, $H^7$), 2.67 (s, 6H, $CH_3$). $^{13}$C{$^1$H} NMR (100 MHz, $CDCl_3$) $\delta$, ppm: 141.6 ($C^{4a}$, $C^{4b}$), 130.9 ($C^3$, $C^6$), 130.8 ($C^2$, $C^7$), 127 ($C^1$, $C^8$), 125.9 ($C^{8a}$, $C^{10a}$), 122.9 ($C^4$, $C^5$), 115.3 ($C^9$, $C^{10}$), 115.2 (CN), 22.4 ($CH_3$). Full assignment of the $^1$H and $^{13}$C NMR spectra was successfully achieved by means of $^1$H–$^{13}$C HSQC and $^1$H–$^{13}$C HMBC measurements (See the Supporting Information, Fig. S2). HRMS (ESI$^+$), *m/z*: 257.1073 $[M+H]^+$, 279.0893 $[M+Na]^+$. $C_{18}H_{13}N_2$ calcd. *m/z*: 257.1079 $[M+H]^+$, $C_{18}H_{12}N_2Na$ calcd. *m/z*: 279.0898. IR spectrum (KBr, selected bands, $cm^{-1}$): 2920 w $\nu$($C_{sp3}$–H), 2226 s $\nu$(C≡N), 1618 s $\nu$($CC_{Ar}$).

*2.2.9. 3,6-Dimethoxyphenanthrene-9,10-dicarbonitrile (**7**)*

Yield: 34 mg (23%), beige powder, mp = 241–242 °C. $^1$H NMR (400 MHz, $CDCl_3$) $\delta$, ppm: 8.30 (d, $^3J$ = 8.8 Hz, 2H, $H^1$, $H^8$), 7.97 (d, $^4J$ = 2.4 Hz 2H, $H^4$, $H^5$), 7.48 (dd, $^3J$ = 8.8 Hz, $^4J$ = 2.4 Hz, 2H, $H^2$, $H^7$), 4.10 (s, 6H, $OCH_3$). $^1$H NMR (400 MHz, DMSO-$d_6$) $\delta$, ppm: 8.38 (d, $^4J$ = 2.0 Hz, 2H, $H^4$, $H^5$), 8.18 (d, $^3J$ = 8.8 Hz, 2H, $H^1$, $H^8$), 7.63 (dd, $^3J$ = 8.8 Hz, $^4J$ = 2.0 Hz, 2H, $H^2$, $H^7$), 4.10 (s, 6H, $OCH_3$). $^{13}$C{$^1$H} NMR (100 MHz, $CDCl_3$) $\delta$, ppm: 161.3, 132.5, 129.1, 122.6, 119.0, 115.8, 113.6, 105.3, 55.6 ($OCH_3$). HRMS (ESI$^+$), *m/z*: 289.0999 $[M+H]^+$, 311.0822 $[M+Na]^+$. $C_{18}H_{13}N_2O_2$ calcd. *m/z*: 289.0977, $C_{18}H_{12}N_2O_2Na$ calcd. *m/z*: 311.0796. IR spectrum (KBr, selected bands, $cm^{-1}$): 2980 w $\nu$($C_{sp3}$–H), 2226 s $\nu$(C≡N), 1616, 1510 s $\nu$($CC_{Ar}$).

### 2.3. Crystallography

The crystals of **2**, **6**, and **7** were obtained by a slow evaporation of solvent at room temperature. Crystals of compounds **2**, **6**, and **7** were immersed in cryo-oil, mounted in a nylon loop, and analysed at a temperature of 100 K. The X-ray diffraction data were collected on an Agilent Technologies Excalibur Eos and Supernova Atlas diffractometers. The temperature for all experiments was kept at 100 K. The structures have been solved by the direct methods and refined by means of the SHELXL–97 [28] program incorporated in the OLEX$^2$ program package [29]. The carbon-bound H atoms were placed in calculated positions and were included in the refinement in the 'riding' model approximation, with $U_{iso}$(H) set to 1.5$U_{eq}$(C) and C–H 0.96 Å for $CH_3$ groups, $U_{iso}$(H) set to 1.2$U_{eq}$(C) and C–H 0.93 Å for the CH groups, and $U_{iso}$(H) set to 1.2$U_{eq}$(N) and N–H 0.86 Å for the NH groups. Empirical absorption correction was applied in CrysAlisPro program complex [30] using spherical harmonics, implemented in SCALE3 ABSPACK scaling algorithm.

The crystallographic details and refinement parameters are summarized in Table 1. The crystallographic details are given in Fig. S3 of the Supporting Information. Crystal data have been deposited at the Cambridge Crystallographic Data Centre (CCDC) with deposition numbers CCDC 1821025, CCDC 1821026, and CCDC 1820117 for **2**, **6**, and **7**, respectively.

### 2.4. Computational details

The single point calculations based on the experimental X-ray geometries of **1**, **2**, **6**, and **7** and full geometry optimization of **1** in the gas phase have been carried out at the DFT level of theory using the M06–2X functional [31] (this functional was parameterized for the main group elements and specifically developed to describe weak dispersion forces and non-covalent interactions) with the help of Gaussian-09 [32] program package. The standard 6–311++G(d,p) basis sets were used for all atoms. No symmetry restrictions have been applied during the geometry optimization.

**Table 1**
Crystallographic data and refinement parameters.

| | **2** | **6** | **7** |
|---|---|---|---|
| Empirical formula | $C_{16}H_6N_2F_2$ | $C_{18}H_{12}N_2$ | $C_{18}H_{12}N_2O_2$ |
| Molecular weight | 264.23 | 256.30 | 288.30 |
| Temp (K) | 100(2) | 100(2) | 100(2) |
| Radiation | CuKα | CuKα | MoKα |
| Crystal system | Monoclinic | Monoclinic | Monoclinic |
| Space group | *Cc* | $P2_1/c$ | $P2_1/c$ |
| *a* (Å) | 3.73677(9) | 11.1090(2) | 7.7888(4) |
| *b* (Å) | 20.2474(5) | 17.7567(3) | 21.946(1) |
| *c* (Å) | 15.6017(4) | 14.0781(3) | 7.8773(4) |
| α (°) | 90 | 90 | 90 |
| β (°) | 94.366(2) | 109.077(2) | 98.517(4) |
| γ (°) | 90 | 90 | 90 |
| *V* (Å$^3$) | 1177.00(5) | 2624.52(9) | 1331.66(11) |
| *Z* | 4 | 8 | 4 |
| $\rho_{calc}$ (mg/mm$^3$) | 1.491 | 1.297 | 1.438 |
| μ ($mm^{-1}$) | 0.946 | 0.601 | 0.096 |
| Total reflections | 5206 | 14792 | 7794 |
| Unique reflections | 1593 | 5113 | 2769 |
| GOOF ($F^2$) | 1.070 | 1.034 | 1.033 |
| $R_{int}$ | 0.0278 | 0.0407 | 0.0268 |
| $R_\sigma$ | 0.0206 | 0.0378 | 0.0377 |
| $R_1$ (all data) | 0.0304 | 0.0568 | 0.0628 |
| w$R_2$ (all data) | 0.0752 | 0.1323 | 0.1109 |
| $R_1$ ($\|F_o\| \geq 4\sigma_F$) | 0.0298 | 0.0456 | 0.0451 |
| w$R_2$ ($\|F_o\| \geq 4\sigma_F$) | 0.0745 | 0.1258 | 0.1016 |

$R_1 = \Sigma||F_o| - |F_c||/\Sigma|F_o|$; $wR_2 = \{\Sigma[w(F_o^2 - F_c^2)^2]/\Sigma[w(F_o^2)^2]\}^{1/2}$; $w = 1/[\sigma^2(F_o^2) + (aP)^2 + bP]$, where $P = (F_o^2 + 2F_c^2)/3$; $s = \{\Sigma[w(F_o^2 - F_c^2)]/(n-p)\}^{1/2}$ where *n* is the number of reflections and *p* is the number of refinement parameters.

The Hessian matrix was calculated analytically for the optimized structure of **1** in order to prove the location of correct minima (no imaginary frequencies). The topological analysis of the electron density distribution with the help of the atoms in molecules (QTAIM) method developed by Bader [33] has been performed by using the Multiwfn program [34]. The Cartesian atomic coordinates of model structures are presented in Table S1 (See the Supporting Information).

## 3. Results and discussion

The fluorescence excitation and emission spectra of **1**–**7** were measured in solution and solid states (Table 2, the Supporting Information, Figs. S4–S5). Strikingly, **7** showed weak fluorescence (the fluorescence quantum yield (ΦF) is less than 1%) in the chloroform solution, but relatively strong fluorescence (ΦF = 46%) in the solid state, whereas **1** and **2** showed opposite emission behaviour (stronger fluorescence in solution than in solid state). **3**–**5** possessed weak fluorescence both in solution and in the solid state, which is related to luminescence quenching by heavy halogen atoms. As well as in the case of compound **7**, **6** exhibits the stronger fluorescence in the solid state (ΦF = 22%) than in the chloroform solution (ΦF = 15%), however, the difference between these two values is not significant. The longest fluorescence lifetime was observed for **7** (11.5 ns in chloroform solution and 25.3 ns in the solid state), while the shortest one belongs to **4** (2.3 ns in chloroform solution and 2.6 ns in the solid state).

The excitation and emission maxima for crystalline **1**–**7** are redshifted compared with chloroform solutions.

To understand the differences in the luminescence properties of phenanthrene-9,10-dicarbonitriles in solution and in the solid state, we have analysed crystal packing patterns of **1**, **2**, **6**, and **7**. Single crystals of **1**, **2**, **6**, and **7** were grown from a dichloromethane solution. The crystal structure of **1** was previously published (CCDC 1443835 [35]). The crystal packing patterns of **1**, **2**, **6**, and **7** (Fig. 3) show that they aggregate by π-stacking with each other; the

**Table 2**
Maximum excitation ($\lambda_{ex}$) and emission ($\lambda_{em}$) wavelengths, Stokes shifts, and fluorescence quantum yields (ΦF) for **1**–**7** in chloroform solution ($c = 5 \cdot 10^{-5}$ M) and in the solid state.

| Compd. | chloroform solution | | | | solid | | | |
|---|---|---|---|---|---|---|---|---|
| | $\lambda_{ex}$ (nm) | $\lambda_{em}$ (nm) | Stokes shift (nm) | $\Phi_F$ (%) | $\lambda_{ex}$ (nm) | $\lambda_{em}$ (nm) | Stokes shift (nm) | $\Phi_F$ (%) |
| **1** | 346 | 395, 416 | 49 | 17 | 387 | 474 | 87 | 11 |
| **2** | 335 | 374, 391, 413 | 39 | 8 | 379 | 464 | 85 | 6 |
| **3** | 347 | 388, 404 | 41 | <1 | 384 | 470 | 86 | <1 |
| **4** | 343 | 412, 426 | 69 | 1 | 380 | 440 | 60 | 2 |
| **5** | 350 | 384, 402, 427 | 34 | 1 | 395 | 458 | 63 | 3 |
| **6** | 343 | 396, 408 | 53 | 15 | 389 | 477 | 88 | 22 |
| **7** | 403 | 440, 463 | 37 | <1 | 433 | 523 | 90 | 46 |

distances between the two stacked layers are 3.4–3.7 Å. The crystal packing pattern of **1** molecules shows that in a stacked column they aggregate by stacking with each other at an angle of 180° plausibly owing to favourable dipole–dipole interaction. The dipole moments of the two molecules exactly eclipse each other, but in the opposite direction. However, it should be noticed, that the stronger non-covalent bonds CN···H(C) assemble the molecules of **1** into the net structure (See the Supporting Information, Fig. S3). In the slip stacked column of **2**, the molecules are oriented in an exactly parallel way (Fig. 3). Also, the intermolecular CN···H(C) and F···H(C) contacts are observed in the crystal structure of **2**. The molecules in the stacked columns of **6** and **7** are rotated relatively to each other. The weak non-covalent CN···H($C_{Ar}$) and CN···H($C_{Me}$) interactions occur between the neighbouring molecules in the crystal of **6**. In **7**, the short contacts CN···H($C_{Ar}$), O···H($C_{Ar}$), and CN···H($C_{MeO}$) are observed (See the Supporting Information, Fig. S3).

Inspection of the crystallographic data also reveals the presence of π-stacking interactions in the crystal structures of **1**, **2**, **6**, and **7**. Taking into consideration that π-stacking interactions often impart important luminescence properties, a detailed computational study of this phenomenon has been performed in this work. In order to confirm or deny the hypothesis on the existence of π-stacking interactions in **1**, **2**, **6**, and **7** and to calculate their energy from theoretical viewpoint, we carried out DFT calculations at the M06–2X/6–311++G(d,p) level of theory and topological analysis of the electron density distribution within the framework of Bader's theory (QTAIM method) [33] for the model systems (Table 3 and Table S1). This approach has already been successfully used by us while studying of different non-covalent interactions in various organic and organometallic or coordination compounds [36–47]. The contour line diagram of the Laplacian distribution $\nabla^2\rho(\mathbf{r})$, bond paths, and selected zero-flux surfaces for the π-stacking interactions in **7** are shown in Fig. 4, corresponding atomic basins of electron density gradient lines map are presented in Fig. S6 (See the Supporting Information). To visualize studied π-stacking

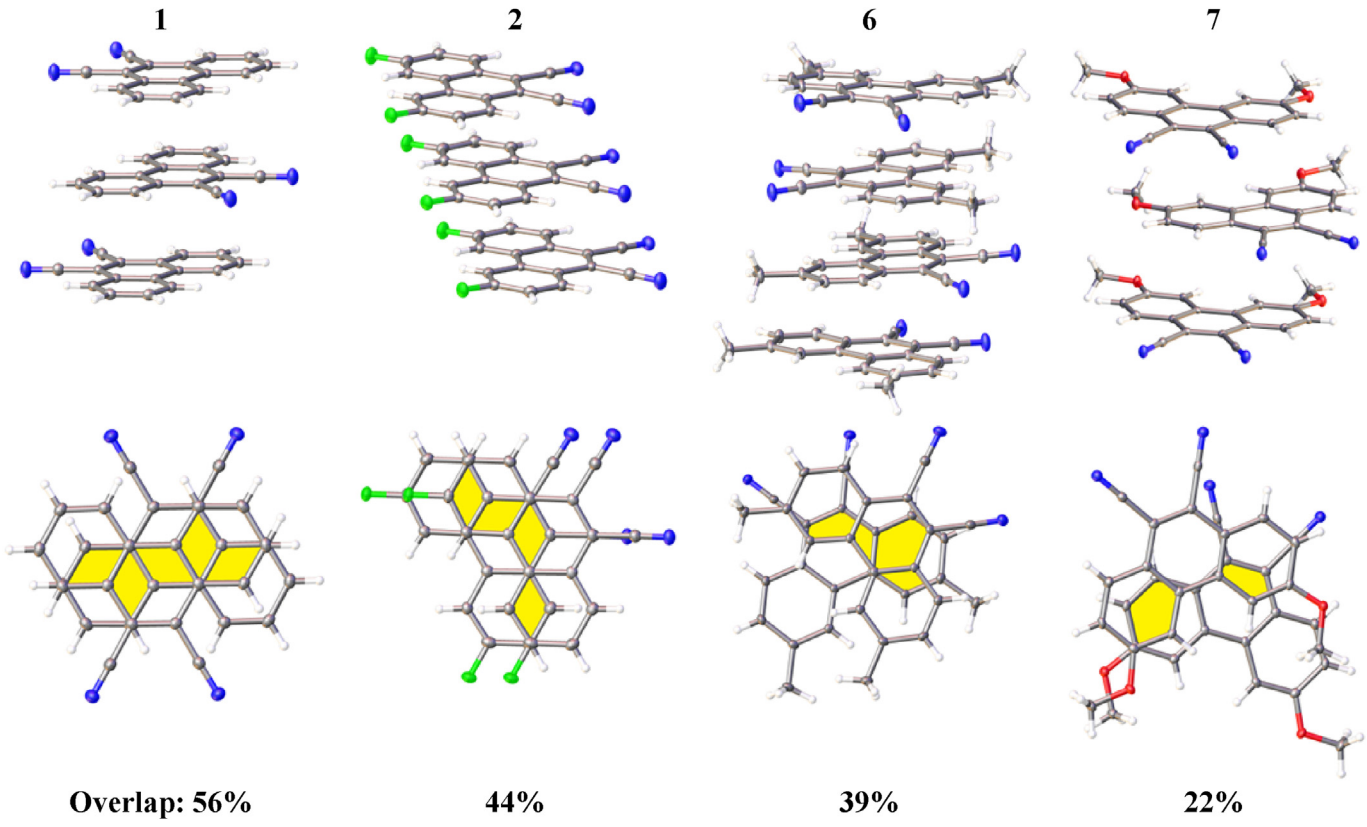


**Fig. 3.** π-Stacking in **1**, **2**, **6**, and **7**.

**Table 3**
Values of the density of all electrons – $\rho(\mathbf{r})$, Laplacian of electron density – $\nabla^2\rho(\mathbf{r})$, energy density – $H_b$, potential energy density – $V(\mathbf{r})$, and Lagrangian kinetic energy – $G(\mathbf{r})$ (a.u.) at the bond critical points (3, –1), corresponding to π-stacking interactions in **1**, **2**, **6**, and **7** as well as energies for appropriate C···C contacts $E_{int}$ (kcal/mol), are defined by two approaches.

| Compd. | ρ(r) | $\nabla^2\rho(r)$ | $H_b$ | V(r) | G(r) | $E_{int}$ [a] | $E_{int}$ [b] |
|---|---|---|---|---|---|---|---|
| **1** | 0.006 | 0.016 | 0.001 | −0.003 | 0.003 | 0.9 | 0.8 |
| **2** | 0.006 | 0.017 | 0.001 | −0.003 | 0.004 | 0.9 | 1.1 |
| **6** | 0.005 | 0.015 | 0.001 | −0.002 | 0.003 | 0.6 | 0.8 |
| **7** | 0.006 | 0.016 | 0.001 | −0.003 | 0.003 | 0.9 | 0.8 |

[a] $E_{int} = -V(\mathbf{r})/2$ [49].
[b] $E_{int} = 0.429G(\mathbf{r})$ [50].

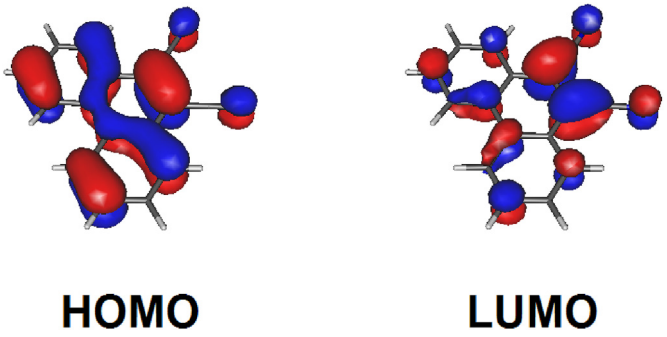


**Fig. 5.** Isosurfaces of HOMO and LUMO for **1**.

interactions, reduced density gradient (RDG) analysis [48] was carried out, and RDG isosurface for **7** was plotted (Fig. 4). The Poincare-Hopf relationship in all cases is satisfactory, thus all critical points have been found.

The QTAIM analysis demonstrates the presence of appropriate bond critical points (BCPs) for the π-stacking interactions in **1**, **2**, **6**, and **7**. The low magnitude of the electron density (0.005–0.006 a.u.), positive values of the Laplacian (0.015–0.017 a.u.), and close to zero positive energy density (0.001 a.u.) in these BCPs are typical for non-covalent interactions. We have defined energies for the C···C contacts responsible for the π-stacking interactions using procedures proposed by Espinosa et al. [49] and Vener et al. [50] (Table 3), and one can state that strength of these non-covalent interactions varies from 0.6 to 1.1 kcal/mol. The balance between the Lagrangian kinetic energy $G(\mathbf{r})$ and potential energy density $V(\mathbf{r})$ at the BCPs (3, –1) reveals the nature of these interactions, if the ratio $-G(\mathbf{r})/V(\mathbf{r}) > 1$ is satisfactory, then the nature of appropriate interaction is purely non-covalent, in case the $-G(\mathbf{r})/V(\mathbf{r}) < 1$ some covalent component takes place [51]. Basing on this criterion one can state that in all cases the covalent contribution in the π-stacking interactions is absent.

The molecules of **6** and **7** seem to behave as independent molecules in the solid state plausibly owing to the unfavourable excited state resonance interaction and thus emit strong fluorescence because each dipolar molecule now is in an inert environment surrounded by other molecules.

For a qualitative estimation of orbital interactions between two stacked molecules, we compared HOMO and LUMO orbitals of phenanthrene-9,10-dicarbonitriles (Fig. 5). The HOMO and LUMO interactions between two stacked molecules may be considered as a model for estimating the excited state resonance interaction. HOMOs of phenanthrene-9,10-dicarbonitriles show larger electron distribution on the phenanthrene fragment, whereas their LUMOs show larger electron distribution on the C9 and C10 atoms of phenanthrene and on the cyano groups. When the HOMO and LUMO of **6** and **7**, in the plane-to-plane stacked mode as in the crystal structure, are compared with respect to the orbital size and symmetry, the orbital overlap is poor; in contrast, more effective orbital overlap is present in the case of **1** (Fig. 3).

Because of the poor orbital interactions between stacked molecules of **6**–**7**, the excited state resonance interaction may become insignificant, which precludes application of Kasha's resonant dimer model to this case. **6**–**7** molecules in the solid state behave independently and thus emit strong fluorescence. Also, poor emission behaviour of **1** and **2** in the solid state is explained by Kasha's exciton model of parallel transition dipoles. **6** and **7** show strong fluorescence in the solid state, whereas **1** and **2** do not. Analysis of the crystal structures and packing patterns reveals that all compounds show parallel stacking patterns that conform to Kasha's exciton model of parallel transition dipoles. **6**–**7**, however, seem to experience an unfavourable excited state resonance interaction, providing an example of a nonresonant stacked model. Frontier molecular orbital interactions between stacked molecules suggest a different degree of orbital overlapping, offering a clue on the different optical behaviour of compounds **1**–**2** and **6**–**7** in the solid state.

## 4. Conclusion

The influence of dipole-dipole and orbital interactions on the luminescent properties of phenanthrene-9,10-dicarbonitriles in the solid state has been studied. The insertion of different substituents in the phenanthrene molecule leads to varied crystal packing, orbital overlap, and, as a result, to emission from cooperative

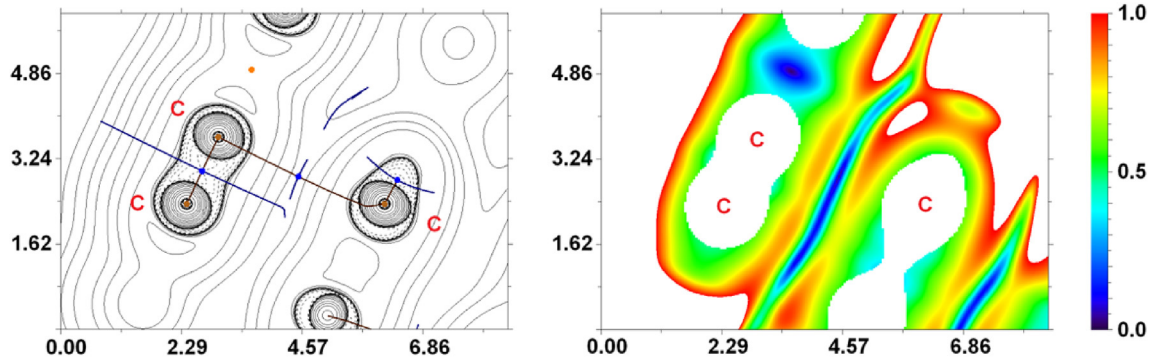


**Fig. 4.** Contour line diagram of the Laplacian distribution $\nabla^2\rho(\mathbf{r})$, bond paths and selected zero-flux surfaces (left) and RDG isosurface (right) referring to π-stacking interactions in **7**. Bond critical points (3, –1) are shown in blue, nuclear critical points (3, –3) – in pale brown, ring critical points (3, +1) – in orange. Length units – Å, RDG isosurface values are given in a.u.

excimer and dipole coupling. The effectiveness of orbital overlap was evaluated by DFT calculation. **6**–**7** demonstrate strong luminescence in the solid state in comparison to the luminescence in solution, but **1**–**2** show the opposite behaviour. The luminescence enhancement in solid **6**–**7** is explained by poor orbital interactions in the excited state. To summarize, the dipole-dipole and orbital intermolecular interactions control the excited state characteristics of phenanthrene-9,10-dicarbonitriles in the solid state, which can help to construct new luminescent materials.

## Acknowledgments

This work has been supported by Russian Foundation for Basic Research (project 16-33-60063). We thank the Centre for Optical and Laser Materials Research, Research Centre for X-ray Diffraction Studies, Educational Resource Centre of Chemistry, Centre for Chemical Analysis and Materials Research, and Centre of Magnetic Resonance (all belong to Saint Petersburg State University) for physicochemical measurements.

## Appendix A. Supplementary data

Supplementary data to this article can be found online at https://doi.org/10.1016/j.molstruc.2019.07.036.

## References

[1] H.E. Katz, Z. Bao, S.L. Gilat, Synthetic chemistry for ultrapure, processable, and high-mobility organic transistor semiconductors, Acc. Chem. Res. 34 (2001) 359–369, https://doi.org/10.1021/ar990114j.
[2] K. Walzer, B. Maennig, M. Pfeiffer, K. Leo, Highly efficient organic devices based on electrically doped transport layers, Chem. Rev. 107 (2007) 1233–1271, https://doi.org/10.1021/cr050156n.
[3] N.J. Hestand, F.C. Spano, Expanded theory of H- and J-molecular aggregates: the effects of vibronic coupling and intermolecular charge transfer, Chem. Rev. 118 (2018) 7069–7163, https://doi.org/10.1021/acs.chemrev.7b00581.
[4] W.Z. Yuan, P. Lu, S. Chen, J.W.Y. Lam, Z. Wang, Y. Liu, H.S. Kwok, M. Yuguang, B.Z. Tang, Changing the behavior of chromophores from aggregation-caused quenching to aggregation-induced emission: development of highly efficient light emitters in the solid state, Adv. Mater. 22 (2010) 2159–2163, https://doi.org/10.1002/adma.200904056.
[5] D. Ding, K. Li, B. Liu, B.Z. Tang, Bioprobes based on AIE fluorogens, Acc. Chem. Res. 46 (2013) 2441–2453, https://doi.org/10.1021/ar3003464.
[6] H. Moon, Q.P. Xuan, D. Kim, Y. Kim, J.W. Park, C.H. Lee, H.J. Kim, A. Kawamata, S.Y. Park, K.H. Ahn, Molecular-shape-dependent luminescent behavior of dye aggregates: bent versus linear benzocoumarins, Cryst. Growth Des. 14 (2014) 6613–6619, https://doi.org/10.1021/cg501567s.
[7] E.E. Jelley, Spectral absorption and fluorescence of dyes in the molecular state, Nature 138 (1936) 1009–1010, https://doi.org/10.1038/1381009a0.
[8] G. Scheibe, Reversible polymerisation als ursache neuartiger absorptionsbanden von Farbstoffen, Kolloid Z. 82 (1938) 1–14, https://doi.org/10.1007/BF01509409.
[9] A. Liess, A. Lv, A. Arjona-Esteban, D. Bialas, A.M. Krause, V. Stepanenko, M. Stolte, F. Würthner, Exciton coupling of merocyanine dyes from H- to J-type in the solid state by crystal engineering, Nano Lett. 17 (2017) 1719–1726, https://doi.org/10.1021/acs.nanolett.6b04995.
[10] A.V. Kulinich, A.A. Ishchenko, Merocyanine dyes: synthesis, structure, properties and applications, Russ. Chem. Rev. 78 (2009) 141–164, https://doi.org/10.1070/rc2009v078n02abeh003900.
[11] S. Özçelik, D.L. Akins, Superradiance of aggregated thiacarbocyanine molecules, J. Phys. Chem. B 103 (2002) 8926–8929, https://doi.org/10.1021/jp991627a.
[12] T. Kaiser, V. Stepanenko, F. Würthner, Fluorescent J-aggregates of core-substituted perylene bisimides: Studies on structure-property relationship, nucleation-elongation mechanism, and sergeants-and-soldiers principle, J. Am. Chem. Soc. 131 (2009) 6719–6732, https://doi.org/10.1021/ja900684h.
[13] S. Ghosh, X.Q. Li, V. Stepanenko, F. Würthner, Control of H- and J-type π stacking by peripheral alkyl chains and self-sorting phenomena in perylene bisimide homo- and heteroaggregates, Chem. Eur J. 14 (2008) 11343–11357, https://doi.org/10.1002/chem.200801454.
[14] S. Yagai, T. Seki, T. Karatsu, A. Kitamura, F. Würthner, Transformation from H-to J-aggregated perylene bisimide dyes by complexation with cyanurates, Angew. Chem. Int. Ed. 47 (2008) 3367–3371, https://doi.org/10.1002/anie.200705385.
[15] C.A. Steinbeck, M. Ernst, B.H. Meier, B.F. Chmelka, Anisotropic optical properties and structures of block copolymer/silica thin films containing aligned porphyrin J-aggregates, J. Phys. Chem. C 112 (2008) 2565–2573, https://doi.org/10.1021/jp075310j.
[16] T. Hinoue, Y. Shigenoi, M. Sugino, Y. Mizobe, I. Hisaki, M. Miyata, N. Tohnai, Regulation of π-stacked anthracene arrangement for fluorescence modulation of organic solid from monomer to excited oligomer emission, Chem. Eur J. 18 (2012) 4634–4643, https://doi.org/10.1002/chem.201103518.
[17] H. Liu, L. Yao, B. Li, X. Chen, Y. Gao, S. Zhang, W. Li, P. Lu, B. Yang, Y. Ma, Excimer-induced high-efficiency fluorescence due to pairwise anthracene stacking in a crystal with long lifetime, Chem. Commun. 52 (2016) 7356–7359, https://doi.org/10.1039/c6cc01993e.
[18] A. Sakai, E. Ohta, Y. Yoshimoto, M. Tanaka, Y. Matsui, K. Mizuno, H. Ikeda, New fluorescence domain "excited multimer" formed upon photoexcitation of continuously stacked diaroylmethanatoboron difluoride molecules with fused π-orbitals in crystals, Chem. Eur J. 21 (2015) 18128–18137, https://doi.org/10.1002/chem.201503132.
[19] S.K. Rajagopal, A.M. Philip, K. Nagarajan, M. Hariharan, Progressive acylation of pyrene engineers solid state packing and colour via C-H···H-C, C-H···O and π-π Interactions, Chem. Commun. 50 (2014) 8644–8647, https://doi.org/10.1039/c4cc01897d.
[20] K. Nagarajan, G. Gopan, R.T. Cheriya, M. Hariharan, Long alkyl side-chains impede exciton interaction in organic light harvesting crystals, Chem. Commun. 53 (2017) 7409–7411, https://doi.org/10.1039/c7cc02322g.
[21] F. Li, N. Gao, H. Xu, W. Liu, H. Shang, W. Yang, M. Zhang, Relationship between molecular stacking and optical properties of 9,10-bis((4-N,N-dialkylamino) styryl) anthracene crystals: the cooperation of excitonic and dipolar coupling, Chem. Eur J. 20 (2014) 9991–9997, https://doi.org/10.1002/chem.201402369.
[22] A. Cook, R. Linstead, Cook and Linstead : phthalocyanines. Part X I . 929 189. Phthalocyanines. Part X I . The preparation, Magnesium (1936) 929–933.
[23] A.M. Afanasenko, D.V. Boyarskaya, I.A. Boyarskaya, T.G. Chulkova, Y.M. Grigoriev, I.E. Kolesnikov, M.S. Avdontceva, T.L. Panikorovskii, A.I. Panin, A.N. Vereshchagin, M.N. Elinson, Structures and photophysical properties of 3,4-diaryl-1H-pyrrol-2,5-diimines and 2,3-diarylmaleimides, J. Mol. Struct. 1146 (2017) 554–561, https://doi.org/10.1016/j.molstruc.2017.06.048.
[24] M.N. Elinson, A.S. Dorofeev, S.K. Feducovich, P.A. Belyakov, G.I. Nikishin, Stereoselective electrocatalytic oxidative coupling of phenylacetonitriles: facile and convenient way to trans-α,β-dicyanostilbenes, Eur. J. Org. Chem. 18 (2007) 3023–3027, https://doi.org/10.1002/ejoc.200601108.
[25] K. Ichimura, S. Watanabe, pH-dependency of photocyclization of diarylfumaronitriles, Bull. Chem. Soc. Jpn. 49 (1976) 2224–2229, https://doi.org/10.1246/bcsj.49.2224.
[26] N. Obata, A. Hamada, T. Takizawa, Photochemical transformation of N-(-toluenesulfonyl)diphenylcyclopropenimine, Tetrahedron Lett. 10 (1969) 3917–3920, https://doi.org/10.1016/S0040-4039(01)88546-4.
[27] E.M. Maya, A.W. Snow, J.S. Shirk, S.R. Flom, R.G.S. Pong, J.H. Callahan, Syntheses, characterization and properties of soluble and liquid phenanthralocyanines, J. Porphyr. Phthalocyanines 06 (2009) 463–475, https://doi.org/10.1142/s1088424602000579.
[28] G.M. Sheldrick, A short history of SHELX, Acta Crystallogr. A. 64 (2008) 112–122, https://doi.org/10.1107/S0108767307043930.
[29] O.V. Dolomanov, L.J. Bourhis, R.J. Gildea, J.A.K. Howard, H. Puschmann, OLEX2 : a complete structure solution, refinement and analysis program, J. Appl. Crystallogr. 42 (2009) 339–341, https://doi.org/10.1107/s0021889808042726.
[30] CrysAlisPro, Agilent Technologies, Version 1.171.36.20 (Release 27 06 2012).
[31] Y. Zhao, D.G. Truhlar, The M06 suite of density functionals for main group thermochemistry, thermochemical kinetics, noncovalent interactions, excited states, and transition elements: two new functionals and systematic testing of four M06-class functionals and 12 other function, Theor. Chem. Acc. 120 (2008) 215–241, https://doi.org/10.1007/s00214-007-0310-x.
[32] M.J. Frisch, G.W. Trucks, H.B. Schlegel, et al., Gaussian 09, Revision C.01, Gaussian Inc., Wallingford CT, 2010.
[33] R.F.W. Bader, Atoms in Molecules: A Quantum Theory, Oxford University Press, 1990.
[34] T. Lu, F. Chen, Multiwfn: a multifunctional wavefunction analyzer, J. Comput. Chem. 33 (2012) 580–592, https://doi.org/10.1002/jcc.22885.
[35] F. Glöcklhofer, M. Lunzer, B. Stöger, J. Fröhlich, A versatile one-pot access to cyanoarenes from ortho- and para-quinones: paving the way for cyanated functional materials, Chem. Eur J. 22 (2016) 5173–5180, https://doi.org/10.1002/chem.201600004.
[36] S.A. Adonin, I.D. Gorokh, A.S. Novikov, P.A. Abramov, M.N. Sokolov, V.P. Fedin, Halogen contacts-induced unusual coloring in BiIII bromide complex: anion-to-cation charge transfer via Br•••Br interactions, Chem. Eur J. 23 (2017) 15612–15616, https://doi.org/10.1002/chem.201703747.
[37] E.V. Andrusenko, E.V. Kabin, A.S. Novikov, N.A. Bokach, G.L. Starova, V.Y. Kukushkin, Metal-mediated generation of triazapentadienate-terminated di- and trinuclear μ2-pyrazolate NiII species and control of their nuclearity, New J. Chem. 41 (2016) 316–325, https://doi.org/10.1039/c6nj02962k.
[38] Z.M. Bikbaeva, D.M. Ivanov, A.S. Novikov, I.V. Ananyev, N.A. Bokach, V.Y. Kukushkin, Electrophilic-nucleophilic dualism of nickel(II) toward Ni···I noncovalent interactions: semicoordination of iodine centers via electron belt and halogen bonding via σ-hole, Inorg. Chem. 56 (2017) 13562–13578, https://doi.org/10.1021/acs.inorgchem.7b02224.
[39] Z.M. Bikbaeva, A.S. Novikov, V.V. Suslonov, N.A. Bokach, V.Y. Kukushkin, Metal-mediated reactions between dialkylcyanamides and acetamidoxime generate unusual (nitrosoguanidinate)nickel(II) complexes, Dalton Trans. 46

(2017) 10090–10101, https://doi.org/10.1039/c7dt01960b.
[40] D.M. Ivanov, A.S. Novikov, G.L. Starova, M. Haukka, V.Y. Kukushkin, A family of heterotetrameric clusters of chloride species and halomethanes held by two halogen and two hydrogen bonds, CrystEngComm 18 (2016) 5278–5286, https://doi.org/10.1039/c6ce01179a.
[41] D.M. Ivanov, Y.V. Kirina, A.S. Novikov, G.L. Starova, V.Y. Kukushkin, Efficient π-stacking with benzene provides 2D assembly of trans-[PtCl2(p-CF3C6H4CN)2], J. Mol. Struct. 1104 (2016) 19–23, https://doi.org/10.1016/j.molstruc.2015.09.027.
[42] D.M. Ivanov, M.A. Kinzhalov, A.S. Novikov, I.V. Ananyev, A.A. Romanova, V.P. Boyarskiy, M. Haukka, V.Y. Kukushkin, H2C(X)-X···X- (X = Cl, Br) halogen bonding of dihalomethanes, Cryst. Growth Des. 17 (2017) 1353–1362, https://doi.org/10.1021/acs.cgd.6b01754.
[43] K.I. Kulish, A.S. Novikov, P.M. Tolstoy, D.S. Bolotin, N.A. Bokach, A.A. Zolotarev, V.Y. Kukushkin, Solid state and dynamic solution structures of O-carbamidine amidoximes gives further insight into the mechanism of zinc(II)-mediated generation of 1,2,4-oxadiazoles, J. Mol. Struct. 1111 (2016) 142–150, https://doi.org/10.1016/j.molstruc.2016.01.038.
[44] A.A. Melekhova, A.S. Novikov, K.V. Luzyanin, N.A. Bokach, G.L. Starova, V.V. Gurzhiy, V.Y. Kukushkin, Tris-isocyanide copper(I) complexes: synthetic, structural, and theoretical study, Inorg. Chim. Acta 434 (2015) 31–36, https://doi.org/10.1016/j.ica.2015.05.002.
[45] A.S. Mikherdov, M.A. Kinzhalov, A.S. Novikov, V.P. Boyarskiy, I.A. Boyarskaya, D.V. Dar'In, G.L. Starova, V.Y. Kukushkin, Difference in energy between two distinct types of chalcogen bonds drives regioisomerization of binuclear (diaminocarbene)PdII complexes, J. Am. Chem. Soc. 138 (2016) 14129–14137, https://doi.org/10.1021/jacs.6b09133.
[46] K. Kolari, J. Sahamies, E. Kalenius, A.S. Novikov, V.Y. Kukushkin, M. Haukka, Metallophilic interactions in polymeric group 11 thiols, Solid State Sci. 60 (2016) 92–98, https://doi.org/10.1016/j.solidstatesciences.2016.08.005.
[47] T.V. Serebryanskaya, A.S. Novikov, P.V. Gushchin, M. Haukka, R.E. Asfin, P.M. Tolstoy, V.Y. Kukushkin, Identification and H(D)-bond energies of C-H(D)···Cl interactions in chloride-haloalkane clusters: a combined X-ray crystallographic, spectroscopic, and theoretical study, Phys. Chem. Chem. Phys. 18 (2016) 14104–14112, https://doi.org/10.1039/c6cp00861e.
[48] E.R. Johnson, S. Keinan, P. Mori-Sánchez, J. Contreras-García, A.J. Cohen, W. Yang, Revealing noncovalent interactions, J. Am. Chem. Soc. 132 (2010) 6498–6506, https://doi.org/10.1021/ja100936w.
[49] E. Espinosa, E. Molins, C. Lecomte, Hydrogen bond strengths revealed by topological analyses of experimentally observed electron densities, Chem. Phys. Lett. 285 (1998) 170–173, https://doi.org/10.1016/S0009-2614(98)00036-0.
[50] M.V. Vener, A.N. Egorova, A.V. Churakov, V.G. Tsirelson, Intermolecular hydrogen bond energies in crystals evaluated using electron density properties: DFT computations with periodic boundary conditions, J. Comput. Chem. 33 (2012) 2303–2309, https://doi.org/10.1002/jcc.23062.
[51] E. Espinosa, I. Alkorta, J. Elguero, E. Molins, From weak to strong interactions: a comprehensive analysis of the topological and energetic properties of the electron density distribution involving X-H···F-Y systems, J. Chem. Phys. 117 (2002) 5529–5542, https://doi.org/10.1063/1.1501133.